Fracture Toughness of Polyamide 6/Maleated Ethylene–Propylene–Diene Terpolymer Rubber/Nano Calcium Carbonate Ternary Composites According to Essential Work of Fracture Analysis

Li-Dan Fu, Si Chen, Yong-Jie Wang, Xiao-Dong Wang, Xu Wang

College of Chemical Engineering and Materials Science, Zhejiang University of Technology, Hangzhou, Zhejiang 310014, People's Republic of China

Received 23 January 2010; accepted 3 September 2010
DOI 10.1002/app.33344
Published online 12 January 2011 in Wiley Online Library (wileyonlinelibrary.com).

ABSTRACT: Polyamide 6 (PA6)/maleated ethylene–propylene–diene terpolymer rubber/nano calcium carbonate ternary composites were prepared. The effect of the compounding route on the morphology, toughness, and fracture behavior of the ternary composites were investigated by scanning electron microscopy, Charpy impact testing, and essential work of fracture (EWF) testing. The construction of sandbag microstructure particles in PA6 matrix was crucial to the toughness of the ternary composites. The Charpy impact strength and the specific essential work of fracture (w_e) of the ternary composites with a sandbag microstructure were 137.9 and 71.4% higher, respectively, than those of the ordinary ternary composites with a separated dispersion microstructure. The observation of the fracture surface after EWF testing indicated that the improvement of w_e was attributed to the sandbag microstructure particles; this structure was more effective for resisting the growth of cracks; meanwhile, the influence of the amount of fibrillation on the nonspecific essential work of fracture, including the nonspecific essential work of fracture before yielding and that in the necking–tearing stage, was insignificant. © 2011 Wiley Periodicals, Inc. J Appl Polym Sci 120: 2971–2978, 2011

Key words: fracture; microstructure; nanocomposites; polyamides; toughness

INTRODUCTION

The toughness of semicrystalline polymers, such as polyamide 6 (PA6), can be improved by the addition of rigid particles or elastomers.[1–9] However, the loading of elastomer largely decreases the stiffness of the polymer, and the toughening effect of rigid-particle-filled polymer composites is often poor because of the agglomeration of particles and the poor interfacial adhesion. [1,10]

Recently, it has been suggested that the stiffness of a rubber toughened polymer could be restored by the addition of rigid particle, which results in that the ternary composites containing elastomer and rigid particle could balance the stiffness and toughness.[10–16] However, the mechanical properties of polymer/elastomer/rigid particle ternary composites are generally dependent not only on the composition but also on the morphologies of the elastomers and rigid particles dispersed in the matrix.[14] In previous articles, we reported that sandbag-microstructure-particle-embedded nano calcium carbonate (nano-$CaCO_3$) agglomerated into ethylene–propylene–diene terpolymer (EPDM) particles could be constructed in polymer/elastomer/rigid particle ternary composites. This sandbag structure effectively improved the toughness and maintained the stiffness of polypropylene and PA6. [17,18]

Generally, the toughness of a plastic is characterized by Charpy impact testing or Izod impact testing. These tests are quite useful because of their convenience and simplicity. However, they provide very limited information on the fracture behavior of a material. Moreover, the impact strength is not suitable for some samples, which cannot be fully broken after Charpy impact testing or Izod impact testing.[8,19] Recently, there has been growing interest in the use of essential work of fracture (EWF) testing to understand the toughness and deformation processes that occur in materials.[20–25] The EWF method was proposed by Broberg[26,27] and extended by Mai and coworkers[28–30] to characterize the fracture behavior of plastics. The fracture toughness measured by the EWF method is equivalent to the critical J-integral method; however, the experimental process and data manipulation of the EWF method are more convenient and simple

Correspondence to: X. Wang (wangxu@zjut.edu.cn).
Contract grant sponsor: Nature Science Foundation of China; contract grant number: 50573067.

than J-integral method.[20,29] Although the toughness of PA6/elastomer/rigid particle ternary composites characterized by impact testing have been extensively investigated, evaluation of the fracture behavior with the EWF method is rare, especially for PA6/elastomer/rigid particle ternary composites with a sandbag microstructure.

In this study, the effect of morphology on the fracture behavior of PA6/maleated ethylene–propylene–diene terpolymer (EPDM-*g*-MA)/nano-$CaCO_3$ ternary composites was examined. The morphology of the ternary composites was observed by scanning electron microscopy (SEM), the impact strength was measured by notched Charpy impact testing, the facture behavior was also characterized with the EWF method, and the distribution of fracture energy in different stages was examined.

EXPERIMENTAL

Materials

The PA6 (1013B) was manufactured by UBE Industries, Ltd. (Yamaguchi, Japan) and had a melt flow rate of 16 g/10 min (at 230°C and with a 2.16-kg load). EPDM (Nordel IP 4725P), with an ethylene content of 70 wt %, was manufactured by DuPont Co. (Wilmington, DE). EPDM-*g*-MA (EPA830), with a maleic anhydride content of 0.90 wt %, was supplied by Haiyi Chemical Co., Ltd. (Hangzhou, China). Nano-$CaCO_3$ (Winnofil'SPM, 40–70 nm), coated with fatty acids, was purchased from Solvay S. A. (Brussels, Belgium). In this study, the mixture of EPDM and EPDM-*g*-MA (weight ratio = 20/80) was defined as EPDM-*g*-MA, and the sandbag microstructure particle was constructed with this ratio.[18] PA6/EPDM-*g*-MA/nano-$CaCO_3$ ternary composites with weight ratios of 75/20/5, 70/20/10, 65/20/15, and 60/20/20 were prepared.

Sample preparation

Two types of PA6/EPDM-*g*-MA/nano-$CaCO_3$ ternary composites were prepared via one-step and two-step compounding routes, respectively. For the one-step compounding route, PA6, EPDM-*g*-MA, and nano-$CaCO_3$ were mixed simultaneously in a twin-screw extruder (Nanjing Chengke Machinery Co., Ltd., Nanjing, China), the extrusion zone temperatures were set at 210–220–225–230°C, and then, the extruded pellets were vacuum-dried at 80°C for 5 h and molded into specimens with an injection-molding machine (Haitian Plastics Machinery Ltd., Ningbo, China), the injection zone temperatures were set at 220, 230, and 240°C. For the two-step compounding route, EPDM-*g*-MA and nano-$CaCO_3$ were mixed in a two-roll mill at 160°C for 15 min to get the master batch, and then, the master batch was melt-mixed with pure PA6 in a twin-screw extruder under the same conditions. Subsequently, the extruded pellets were vacuum-dried at 80°C for 5 h and molded into specimens with an injection-molding machine under the same conditions. Before they were mixed, PA6 and nano-$CaCO_3$ were vacuum-dried at 80°C for 5 h.

Charpy impact test

The Charpy impact test was conducted with V-notched [3.2-mm thickness (t)] specimens [length × Width (W) × t = 80 × 10 × 4 mm^3] according to ISO 179–2000 on a Sans ZBC1251-2 impact tester (MTS Systems Co., Ltd., Shenzhen, China) (7.5-J pendulum and 3.8 m/s impact velocity) at 23 ± 2°C. Five specimens were tested to obtain the average impact strength.

EWF test

EWF testing is based on the hypothesis that the total fracture energy (W_f) can be divided into two parts:[23–25] the specific essential work of fracture (W_e) and the nonessential (i.e., plastic) work of fracture (W_p). The former is a surface energy dissipated in the inner fracture process zone (FPZ), whereas the latter is a volumetric energy dissipated in the outer diffuse plastic deformation zone (PDZ). W_f can be written as follows:

$$W_f = W_e + W_p \tag{1}$$

Equation (1) can be further expressed in the terms of specific parameters as follows:

$$w_f = W_f/lt = w_e + \beta w_p l \tag{2}$$

where w_f is the specific total work of fracture, w_e is the specific essential work of fracture associated with FPZ, w_p is the specific nonessential (or plastic) work of fracture associated with PDZ, β is the shape factor of the plastic zone, βw_p is the nonspecific essential work of fracture or the plastic work term that represents the total plastic energy dissipated in the plastic zone, and l is the ligament length.[23–25]

Furthermore, the w_f values for every l can be calculated from a numerical integration of the load–displacement curves.[24] When w_f is plotted as a function of l, the values of w_e and βw_p can be obtained from the y-axis intercept and slope of the w_f–l plots extrapolated to zero l.[20,25] Taking the peak of the load–displacement curve as the cutoff point, W_f can be partitioned into the energy dissipated in the stage

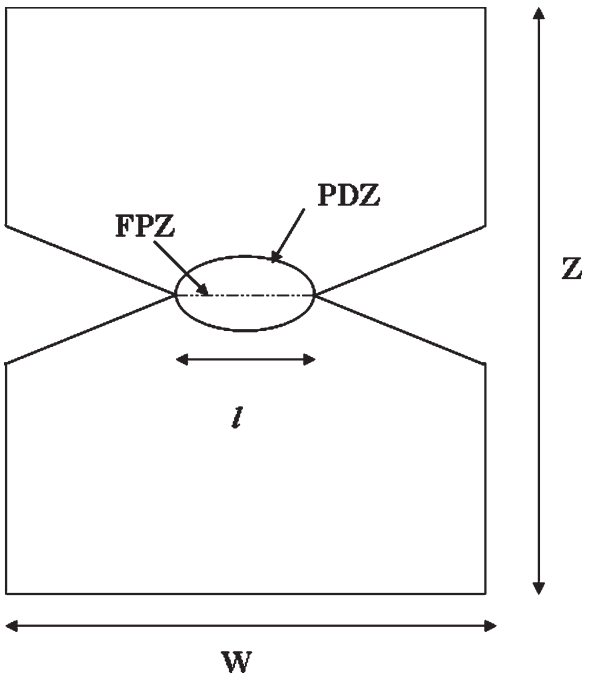

Figure 1 DENT sample used for the EWF test. FPZ = inner fracture process zone; PDZ = outer diffuse plastic deformation zone; Z = length of the DENT sample.

before yielding [or yielding specific work of fracture ($W_{f,y}$)] and the energy dissipated in the necking–tearing stage after yielding [or necking specific work of fracture ($W_{f,n}$)].[24,25] Accordingly, the following equations can be written as

$$w_f = w_{f,y} + w_{f,n} \quad (3)$$

$$w_{f,y} = w_{e,y} + \beta' w_{p,y} l \quad (4)$$

$$w_{f,n} = w_{e,n} + \beta'' w_{p,n} l \quad (5)$$

where $w_{f,y}$ and $w_{f,n}$ is the specific total fracture work before and after yielding in the necking–tearing stage, respectively, $w_{e,y}$ and $w_{e,n}$ are the corresponding specific essential work of fracture, and $\beta' w_{p,y}$ and $\beta'' w_{p,n}$ are the corresponding plastic work terms.[24,25]

The double-edge notched tensile (DENT) specimen (length × W × t = 100 mm × 35 mm × 0.5 mm) was used for the EWF test (Fig. 1), which is similar to the specimens described in the Ref. 25. l was limited in the following range according to European structural integrity society (ESIS) recommendations:[31]

$$3t < l < W/3 \quad (6)$$

EWF testing was conducted on an Instron (4302) universal test machine (Canton, MA), which was equipped with a 500-N load cell at a crosshead speed of 5 mm/min and at 23 ± 2°C, and the load–displacement curves were recorded until breakage of the specimens. The absorbed energy during the fracture process was calculated from the integrated area under the load–displacement curves.

SEM investigation

The microstructure of the specimens was observed with a Hitachi S4700 (II) scanning electron microscope (Hitachi, Japan) with an acceleration voltage of 15 kV. To investigate the morphology of EPDM-*g*-MA and nano-$CaCO_3$ in the PA6 matrix, the specimens were cryogenically fractured along the direction perpendicular to the flow direction in liquid nitrogen and were then immersed in boiling toluene for 1 h to preferentially etch the EPDM-*g*-MA phase. To investigate the fracture structures after EWF testing, fresh specimens for EWF testing were used. The

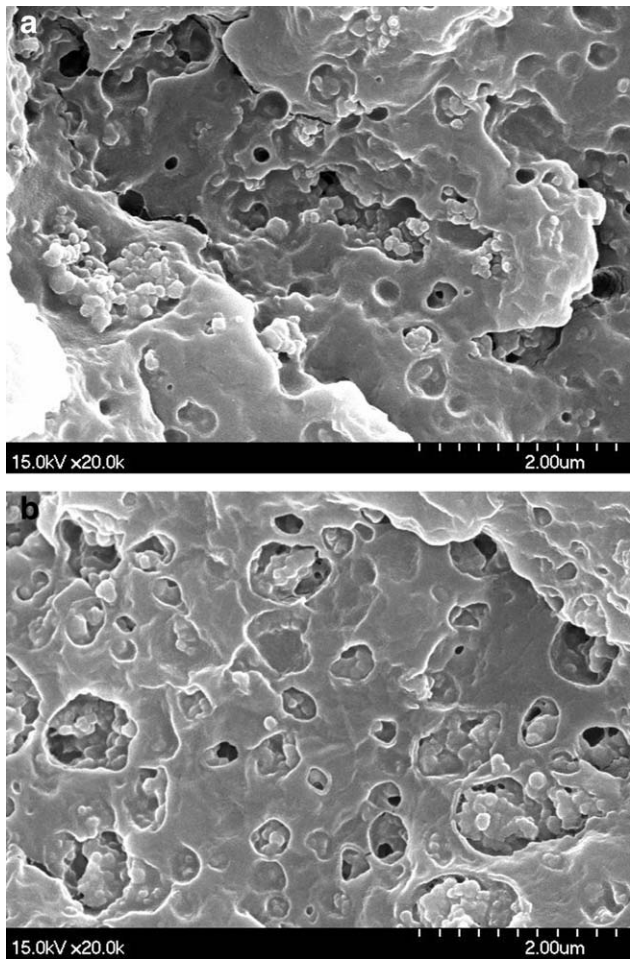

Figure 2 SEM images of the etched cryofractured surfaces of the PA6/EPDM-*g*-MA/nano-$CaCO_3$ (60/20/20) ternary composites prepared via two compounding routes: (a) one-step route and (b) two-step route.

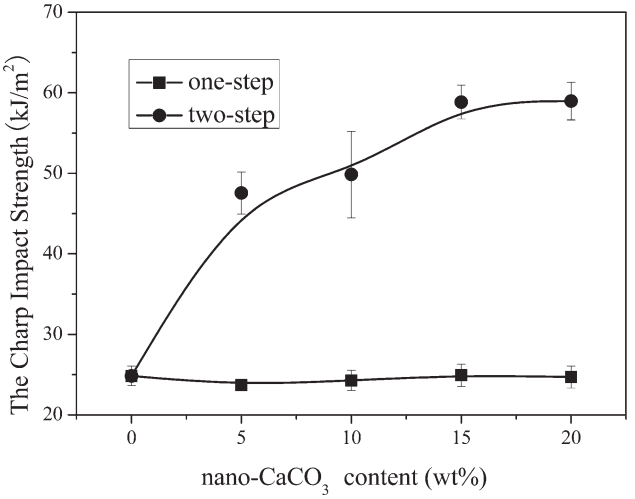

Figure 3 Effect of the nano-$CaCO_3$ content on the Charpy impact strength of the PA6/EPDM-*g*-MA/nano-$CaCO_3$ ternary composites prepared via two compounding routes.

etched fracture surfaces and the fracture surfaces after EWF testing were coated with Au before they were investigated.

RESULTS AND DISCUSSION

Morphology

Figure 2 is SEM image of the etched cryofractured surface of the PA6/EPDM-*g*-MA/nano-$CaCO_3$ (60/20/20) ternary composites prepared via one-step and two-step compounding route. The dark holes in the SEM images are the domains where the EPDM-*g*-MA particles were selectively removed. The smaller bright domains with irregular geometry are nano-$CaCO_3$ agglomerates.

For the PA6/EPDM-*g*-MA/nano-$CaCO_3$ ternary composites prepared via a one-step process, large spheroidal EPDM-*g*-MA particles and small nano-$CaCO_3$ agglomerates were separately dispersed in the PA6 matrix; this indicated that a separated dispersion microstructure was probably formed [Fig. 2(a)]. For the PA6/EPDM-*g*-MA/nano-$CaCO_3$ ternary composites prepared via a two-step process, as shown in Figure 2(b), the nano-$CaCO_3$ agglomerates were selectively embedded in the EPDM-*g*-MA particles. In our previous study, the morphology with rigid-particle agglomerates embedded in the elastomer was defined as a sandbag microstructure.[17,18] SEM images indicated that the morphology of the polymer/elastomer/rigid particles ternary composites was strongly dependent on the compounding route.

Charpy impact testing

Figure 3 shows the effect of the nano-$CaCO_3$ content on the Charpy impact strength of the PA6/EPDM-*g*-MA/nano-$CaCO_3$ ternary composites prepared via two compounding routes. The Charpy impact strength of the ternary composites, prepared via a two-step compounding route, was remarkably enhanced. However, for the ternary composites prepared via the one-step compounding route, little improvement in the Charpy impact strength was observed. When the nano-$CaCO_3$ content was 20 wt %, the Charpy impact strength of the ternary composites prepared via the two-step compounding route was 137.9% higher than that of the ternary composites prepared via the one-step compounding route. Because the mechanical properties of the polymer/elastomer/rigid particles ternary composites largely depended on the morphology, this indicated that sandbag microstructure particles were crucial for the toughness of the ternary composites. This was conformed in our previous studies, for which we also reported that sandbag microstructure particles effectively dissipated the impact energy to improve the toughness.[17,18]

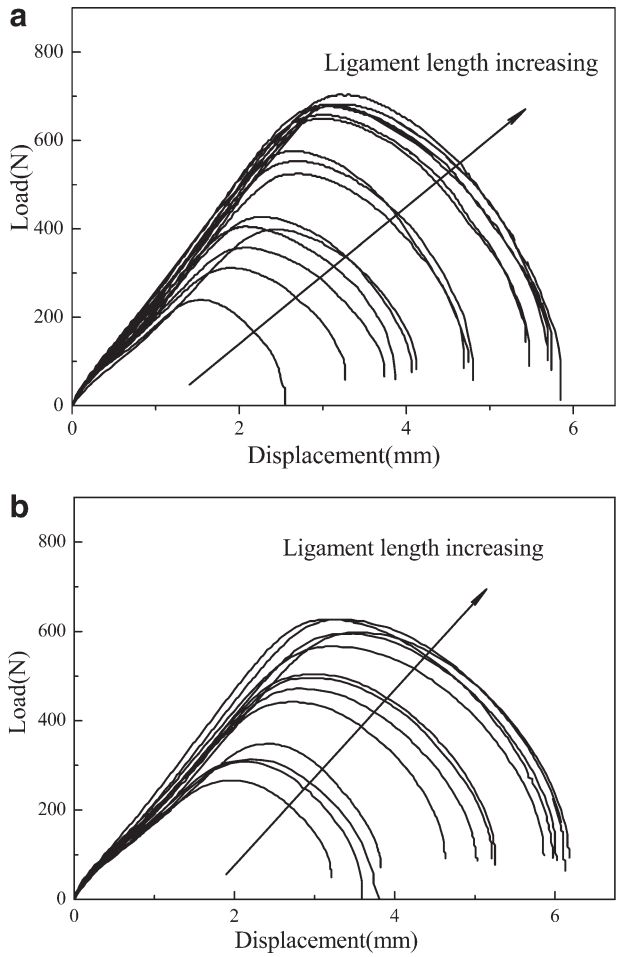

Figure 4 Load–displacement curves of the PA6/EPDM-*g*-MA/nano-$CaCO_3$ (60/20/20) ternary composites with different *l* values: (a) separated dispersion microstructure and (b) sandbag microstructure.

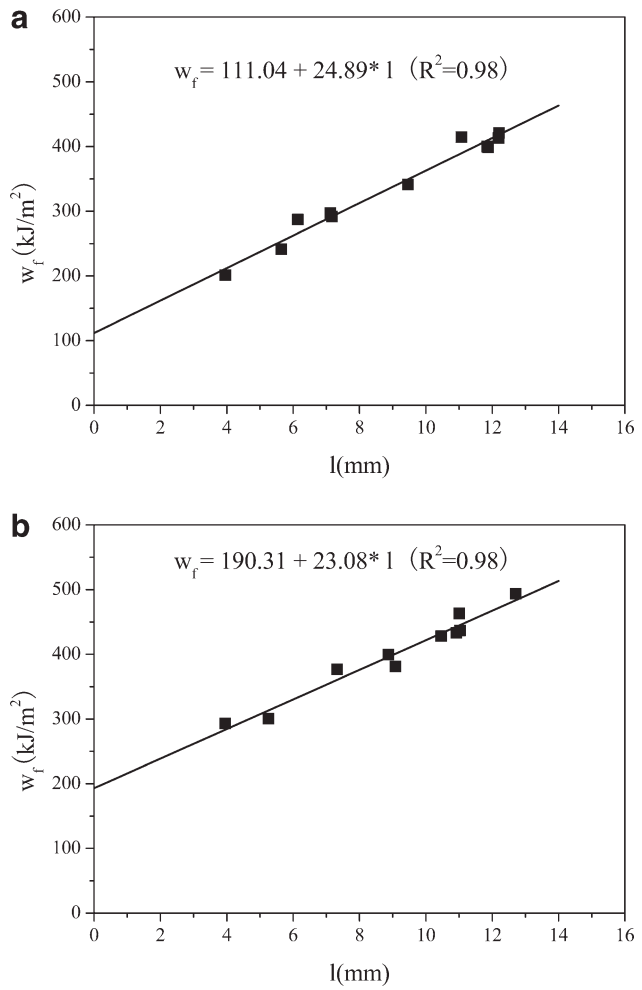

Figure 5 Specific work of fracture versus *l* for PA6/EPDM-*g*-MA/nano-$CaCO_3$ (60/20/20) ternary composites: (a) separated dispersion microstructure and (b) sandbag microstructure.

EWF testing

Figure 4 shows the load–displacement curves of two types of PA6/EPDM-*g*-MA/nano-$CaCO_3$ ternary composites (60/20/20) with different *l* values. Clearly, the load–displacement curves were very similar, and all of the specimens showed a ductile fracture model. At first, the load increased quickly with a slight increase in the displacement, and then, with increasing displacement, after yielding, the load decreased slowly and smoothly until the specimen broke. The maximum load, the displacement to breakage, and the area under the curves increased regularly with increasing *l*, indicating that the mode of fracture was independent of *l*, which further ensured the validity of the EWF method.[25] The fracture parameters for the PA6/EPDM-*g*-MA/nano-$CaCO_3$ ternary composites were obtained by the load–displacement curves. The plot of w_f, $w_{f,y}$, and $w_{f,n}$ against *l* of the PA6/EPDM-*g*-MA/nano-$CaCO_3$ ternary composites with a separated dispersion microstructure and sandbag microstructure are shown in Figures 5–7, respectively. The fracture parameters obtained from the interception and slope of w_f–*l*, $w_{f,y}$–*l*, and $w_{f,n}$–*l* plots extrapolated to zero *l* are listed in Table I. Figures 5–7 present good linear relationships for all of the specimens; this was confirmed by the high linear regression coefficient ($R^2 > 0.97$) in most cases.

w_e is a material constant used to characterize the fracture toughness, which is only dependent on *t* and independent of the geometry of the specimen.[22,25] As shown in Table I, the value of w_e of the PA6/EPDM-*g*-MA/nano-$CaCO_3$ ternary composites with a sandbag microstructure was 71.4% higher than that of the composites with a separated dispersion microstructure; this indicated that the fracture toughness, that is, the crack resistance, was improved.[25] The results suggest that w_e was sensitive to the morphology of the ternary composites.

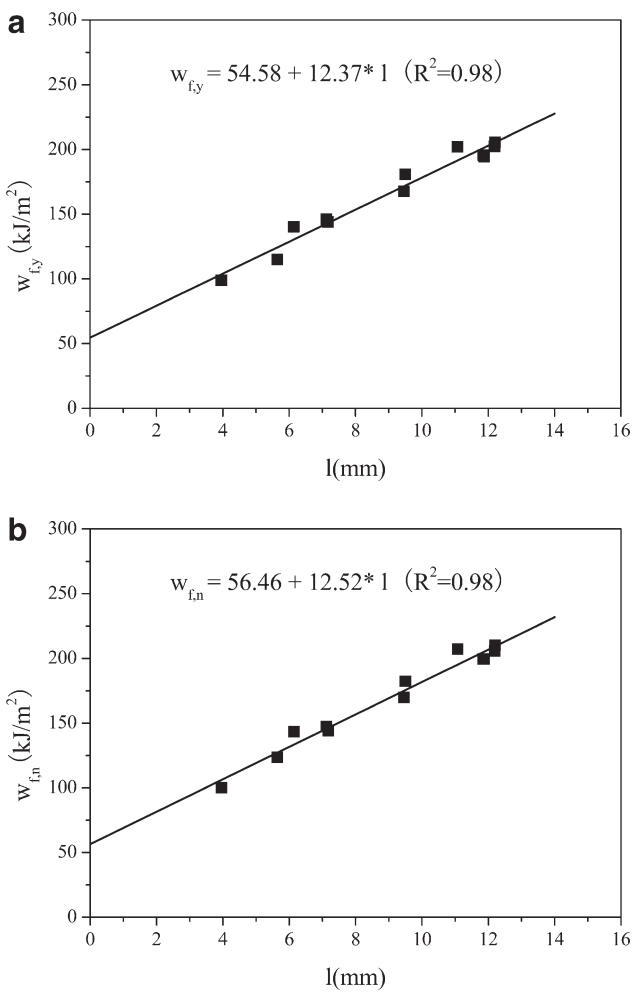

Figure 6 Yielding and necking specific work of fracture versus *l* for PA6/EPDM-*g*-MA/nano-$CaCO_3$ (60/20/20) ternary composites with a separated dispersion microstructure: (a) yielding and (b) necking–tearing.

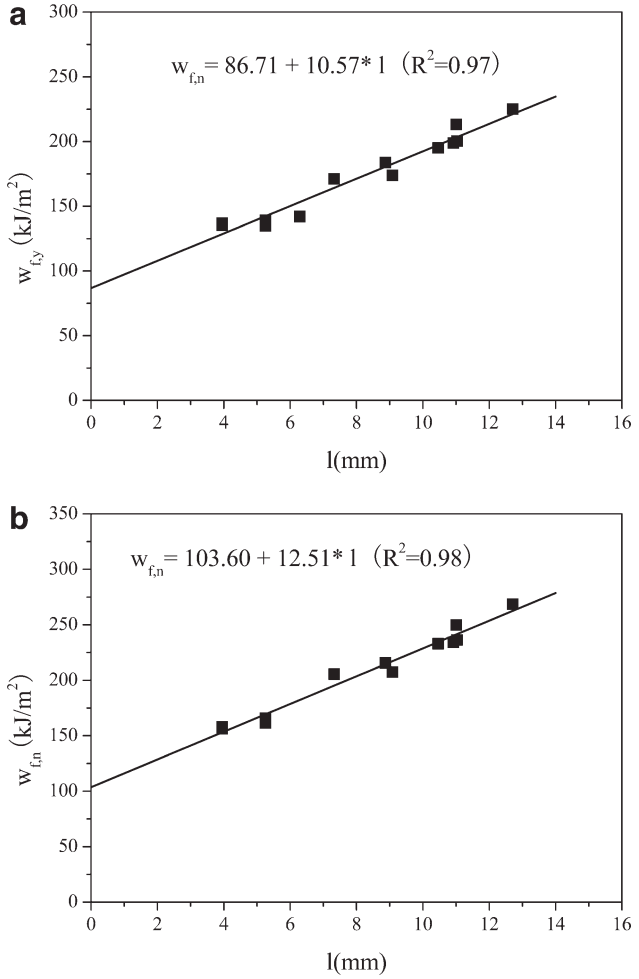

Figure 7 Yielding and necking specific work of fracture against l for PA6/EPDM-*g*-MA/nano-$CaCO_3$ (60/20/20) ternary composites with a sandbag microstructure: (a) yielding and (b) necking–tearing.

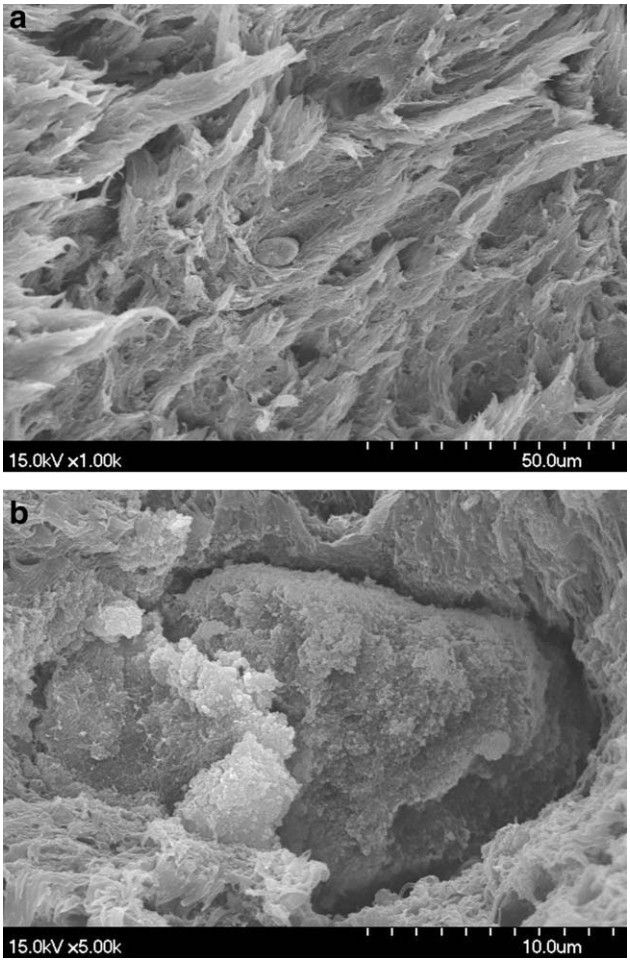

Figure 8 SEM images of the fracture surface of the PA6/EPDM-*g*-MA/nano-$CaCO_3$ (60/20/20) ternary composites with a separated dispersion microstructure after EWF testing at two levels of magnification: (a) 1000 and (b) 5000×.

As shown by the values listed in Table I, clearly, the values of $w_{e,y}$ and $w_{e,n}$ of the PA6/EPDM-*g*-MA/nano-$CaCO_3$ ternary composites with a sandbag microstructure were 58.9 and 83.5% higher than those of the composites with a separated dispersion microstructure, respectively; this indicated that the crack resistance in the whole fracture process both before yielding and in the necking–tearing stage and the fracture toughness were improved, especially in the necking–tearing stage. For the ternary composites with a sandbag microstructure, the value of $w_{e,n}$ was 18.8% higher than $w_{e,y}$. Furthermore, w_e in the whole fracture process of the ternary composites with a sandbag microstructure particles was more determined by $w_{e,n}$.

TABLE I
Fracture Parameters for PA6/EPDM-g-MA/nano-CaCO3 Ternary Composites (60/20/20) with Separated Dispersion Microstructure and Sandbag Microstructure

	Separated dispersion microstructure	Sandbag microstructure
w_e (kJ/m^2)	111.04	190.31
βw_p (MJ/m^2)	24.89	23.08
$w_{e,y}$ (kJ/m^2)	54.58	86.71
$w_{e,n}$ (kJ/m^2)	56.46	103.60
$\beta w_{p,y}$ (MJ/m^2)	12.37	10.57
$\beta w_{p,n}$ (MJ/m^2)	12.52	12.51

On the other hand, Table I shows that the morphology of the ternary composites did not significantly affect the plastic energy consumption [βw_p; including the nonspecific essential work of fracture before yielding ($\beta w_{p,y}$) and nonspecific essential work of fracture in the necking–tearing stage ($\beta w_{p,n}$)].

To understand the fracture parameters obtained, the fracture surfaces of the DENT specimens after EWF testing were observed by SEM. Both voids and the tearing of fibrils, or fibrillation, were observed in the PA6/EPDM-*g*-MA/nano-$CaCO_3$ ternary composites with separated dispersion microstructure (Fig. 8) and the ternary composites with the sandbag microstructure (Fig. 9). Figure 8 shows that several

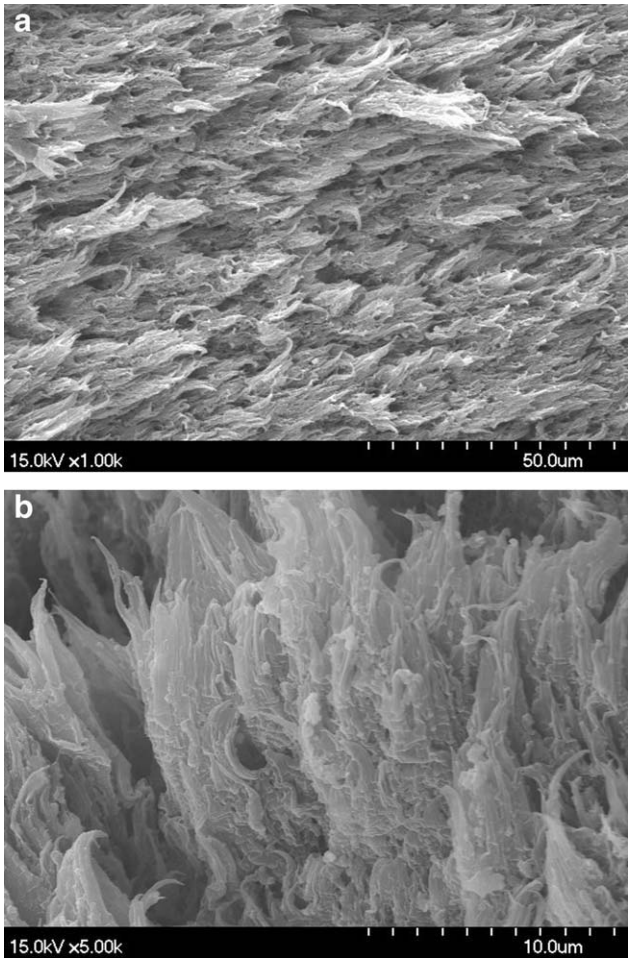

Figure 9 SEM images of the fracture surface of the PA6/EPDM-*g*-MA/nano-$CaCO_3$ (60/20/20) ternary composites with a sandbag microstructure after EWF testing at two levels of magnification: (a) 1000 and (b) 5000×.

voids were formed at large nano-$CaCO_3$ agglomerates; however, large nano-$CaCO_3$ agglomerates were very seldom observed in the ternary composites with the sandbag microstructure, in which small nano-$CaCO_3$ agglomerates were selectively distributed in the fibrils [Fig. 9(b)]. Because large nano-$CaCO_3$ agglomerates could act as void nuclei, this poor dispersion of nano-$CaCO_3$ particles decreased the fracture toughness (w_e, the crack resistance), and the sandbag microstructure contributed to the important improvement in w_e.[32] This indicated that the sandbag microstructure particles were more effective in resisting the growth of cracks than the larger nano-$CaCO_3$ agglomerates.

On the other hand, the difference between the fracture features of the ternary composites with the sandbag microstructure and the separated dispersion microstructure was the fibrillation (Figs. 8 and 9). The amount of fibrillation in the ternary composites with the sandbag microstructure (Fig. 9) was greater than that in the ternary composites with the separated dispersion microstructure (Fig. 8). Bureau et al.[32] reported that the amount of fibrillation determines the plastic energy consumption, that is, βw_p. However, in our study, the discrepancy between βw_p was small, and the amount of fibrillation had little influence on the plastic energy consumption. This contradiction might have been due to the matrix; in Bureau's work, polypropylene was used as matrix. However, we are not quite sure about this point. There is still a lot of experimentation and discussion to be done to answer this question.

CONCLUSIONS

In this study, two types of morphology were clearly observed in PA6/EPDM-*g*-MA/nano-$CaCO_3$ ternary composites prepared by two compounding routes. Sandbag microstructure particles were constructed via a two-step compounding route. The sandbag microstructure particles were crucial for the toughness of the ternary composites and the Charpy impact strength, and the fracture toughness (w_e) values of the ternary composites with the sandbag microstructure were 137.9 and 71.4% higher than that with the separated dispersion microstructure, respectively. The improvement in w_e was related to the sandbag microstructure particles, which were more effective in resisting the growth of cracks. The changes in βw_p, $\beta w_{p,y}$, and $\beta w_{p,n}$ in these two types of ternary composites was relatively small; this suggested that the amount of fibrillation had little influence on the plastic energy consumption.

The authors are thankful to Yang Ming Bo (Sichuan University) for his help with the EWF testing.

References

1. Wilbrink, M. W. L.; Argon, A. S.; Cohen, R. E.; Weinberg, M. Polymer 2001, 42, 10155.
2. Okada, O.; Keskkula, H.; Paul, D. R. J Polym Sci Pol Phys 2004, 42, 1739.
3. Van Puyvelde, P.; Oommen, Z.; Koets, P.; Groeninckx, G.; Moldenaers, P. Polym Eng Sci 2003, 43, 71.
4. Gallego, R.; Garcia-Lopez, D.; Lopez-Quintana, S.; Gobernado-Mitre, I.; Merino, J. C.; Pastor, J. M. Polym Bull 2008, 60, 665.
5. Wang, C.; Su, J. X.; Li, J.; Yang, H.; Zhang, Q.; Du, R. N.; Fu, Q. Polymer 2006, 47, 3197.
6. Burgisi, G.; Paternoster, M.; Peduto, N.; Saraceno, A. J Appl Polym Sci 1997, 66, 777.
7. Yu, Z. Z.; Ke, Y. C.; Ou, Y. C.; Hu, G. H. J Appl Polym Sci 2000, 76, 1285.
8. Kudva, R. A.; Keskkula, H.; Paul, D. R. Polymer 2000, 41, 335.
9. Kayano, Y.; Keskkula, H.; Paul, D. R. Polymer 1997, 38, 1885.
10. Tjong, S. C.; Bao, S. P. J Polym Sci Part B: Polym Phys 2005, 43, 585.
11. Balamurugan, G. P.; Maiti, S. N. Polym Test 2008, 27, 752.
12. Kelnar, I.; Kotek, J.; Kapralkova, L.; Hromadkova, J.; Kratochvil, J. J Appl Polym Sci 2006, 100, 1571.

13. Ma, C. G.; Mai, Y. L.; Rong, M. Z.; Ruan, W. H.; Zhang, M. Q. Compos Sci Technol 2007, 67, 2997.
14. Zebarjad, S. M.; Sajjadi, S. A.; Tahani, M. J Mater Process Technol 2006, 175, 446.
15. Ou, Y. C.; Guo, T. T.; Fang, X. P.; Yu, Z. Z. J Appl Polym Sci 1999, 74, 2397.
16. Wang, X.; Xu, K. J.; Xu, X. B.; Park, S. J.; Kim, S. J Appl Polym Sci 2009, 113, 2485.
17. Wang, X.; Sun, J.; Huang, R. J Appl Polym Sci 2006, 99, 2268.
18. Wang, X.; Wang, X. D.; Xu, X. B. J Macromol Sci Phys 2009, 48, 1212.
19. Tjong, S. C.; Xu, S. A.; Mai, Y. W. Mater Sci Eng A 2003, 347, 338.
20. Poon, W. K. Y.; Ching, E. C. Y.; Cheng, C. Y.; Li, R. K. Y. Polym Test 2001, 20, 395.
21. Lievana, E.; Bernal, C.; Frontini, P. Polym Eng Sci 2004, 44, 1707.
22. Gong, G.; Xie, B. H.; Yang, W.; Li, Z. M.; Zhang, W. Q.; Yang, M. B. Polym Test 2005, 24, 410.
23. Chen, H. B.; Wu, J. S. Macromolecules 2007, 40, 4322.
24. Gamez-Perez, J.; Santana, O.; Martinez, A. B.; Maspoch, M. L. Polym Test 2008, 27, 491.
25. Liu, Y.; Xie, B. H.; Yang, W.; Zhang, W. Q.; Feng, J. M.; Yang, M. B. Polym Test 2007, 26, 388.
26. Broberg, K. B. Int J Fracture1968, 4, 11.
27. Broberg, K. B. J Mech Phys Solids 1971, 19, 407.
28. Mai, Y. W.; Cotterell, B. Int J Fracture 1984, 24, 229.
29. Mai, Y. W.; Cotterell, B.; Horlyck, R.; Vigna, G. Polym Eng Sci 1987, 27, 804.
30. Mai, Y. W.; Cotterell, B. Eng Fract Mech 1985, 21, 123.
31. Clutton E. Testing Protocol for Essential Work of Fracture; European Structural Integrity Society (ESIS) TC-4 Group: Les Diablerets, Switzerland, 1997.
32. Bureau, M. N.; Perrin-Sarazin, F.; Ton-That, M. T. Polym Eng Sci 2004, 44, 1142.